HHS Public Access

Author manuscript

Cancer Immunol Res. Author manuscript; available in PMC 2020 June 01.

Published in final edited form as:

Cancer Immunol Res. 2019 June ; 7(6): 977–989. doi:10.1158/2326-6066.CIR-18-0448.

Differential effects of depleting versus programming tumor-associated macrophages on engineered T cells in pancreatic ductal adenocarcinoma

Ingunn M. Stromnes[1,2,†], **Adam L. Burrack**[1,2], **Ayaka Hulbert**[3,4], **Patrick Bonson**[3,4], **Cheryl Black**[3,4], **J. Scott Brockenbrough**[3], **Jackson F. Raynor**[1,2], **Ellen J. Spartz**[1,2], **Robert H. Pierce**[3,4], **Philip D. Greenberg**[3,4,6,#,†], and **Sunil R. Hingorani**[3,5,6,#,†]

[1]Center for Immunology, University of Minnesota Medical School, Minneapolis, MN 55455;

[2]Department of Microbiology and Immunology, University of Minnesota Medical School, Minneapolis, MN 55455;

[3]Clinical Research Division, Fred Hutchinson Cancer Research Center, Seattle, WA, 98109;

[4]Program in Immunology, Fred Hutchinson Cancer Research Center, Seattle, WA, 98109;

[5]Public Health Sciences Division of the Fred Hutchinson Cancer Research Center, Seattle, WA, 98109;

[6]Division of Medical Oncology, University of Washington School of Medicine, Seattle, WA, 98195

Abstract

Pancreatic ductal adenocarcinoma (PDA) is a lethal malignancy resistant to therapies, including immune checkpoint blockade. We investigated two distinct strategies to modulate tumor-associated macrophages (TAMs) to enhance cellular therapy targeting mesothelin in an autochthonous PDA mouse model. Administration of an antibody to colony-stimulating factor (anti-Csf1R) depleted Ly6C^{low} pro-tumorigenic TAMs and significantly enhanced endogenous T-cell intratumoral accumulation. Despite increasing the number of endogenous T cells at the tumor site, as previously reported, TAM depletion had only minimal impact on intratumoral accumulation and persistence of T cells engineered to express a murine mesothelin-specific T-cell receptor (TCR). TAM depletion interfered with the antitumor activity of the infused T cells in PDA, evidenced by reduced tumor cell apoptosis. In contrast, TAM programming with agonistic anti-CD40 increased both Ly6C^{high} TAMs and the intratumoral accumulation and longevity of TCR-engineered T cells. Anti-CD40 significantly increased the frequency and number of proliferating and granzyme B^{+} engineered T cells, and increased tumor cell apoptosis. However,

[†]**Correspondence:** Ingunn M. Stromnes, Center for Immunology, University of Minnesota, 2101 6th Street, MBB 2-186, Minneapolis, MN 55455, ingunn@umn.edu, Philip D. Greenberg, Fred Hutchinson Cancer Research Center, Program in Immunology, 1100 Fairview Ave N, D3-100, Seattle, WA 98109-1024, pgreen@uw.edu, Sunil R. Hingorani, Fred Hutchinson Cancer Research Center, 1100 Fairview Ave N, M5-C800, Seattle, WA 98109-1024, srh@fhcrc.org.
#Co-senior author

AUTHOR CONTRIBUTIONS: I.M.S., A.L.B., A.H., P.B., C.B., J.R., E.J.S, J.S.B. performed experiments. I.M.S. and A.L.B. analyzed the data and wrote the manuscript. R.H.P. provided histological expertise. P.D.G. and S.R.H. edited the manuscript. I.M.S., P.D.G. and S.R.H. designed and supervised the study.

Conflict of Interest Statement: P.D.G. is a consultant for Juno Therapeutics, a Celgene company, and a consultant and stockholder in FLX Bio, ElpiScience, Immune Design, and NexTech. S.R.H. is a consultant for Halozyme Therapeutics, Inc.

anti-CD40 failed to rescue intratumoral engineered T-cell IFNγ production. Thus, although functional modulation, rather than TAM depletion, enhanced the longevity of engineered T cells and increased tumor cell apoptosis, ultimately, anti-CD40 modulation was insufficient to rescue key effector defects in tumor-reactive T cells. This study highlights critical distinctions between how endogenous T cells that evolve *in vivo*, and engineered T cells with previously acquired effector activity, respond to modifications of the tumor microenvironment.

Keywords

Pancreatic cancer; PDA; T cell; immunotherapy; macrophage

INTRODUCTION

Pancreatic ductal adenocarcinoma (PDA) has a dismal 5-year survival rate of 9% (1,2). The disease is resectable in 10–20% of patients, and aggressive and toxic treatments, including chemotherapy and radiotherapy, are rarely curative. Immunotherapy that augments endogenous immune system activity, such as immune checkpoint blockade, can be effective in other advanced malignancies, yet has not been successful in most PDA patients (3,4). Resistance to immune checkpoint blockade may reflect, in part, too few neoantigens (5). Infusion of T cells engineered to express tumor-specific T-cell receptors (TCRs) or chimeric antigen receptors (CARs) has yielded some therapeutic responses in cancer patients, and may be particularly useful for tumors with few neoantigens. We previously showed (6) that $CD8^+$ T cells engineered to express a high-affinity TCR specific to mesothelin (TCR_{Msln}) infiltrate pancreatic tumors and prolong survival in an autochthonous PDA mouse model (*Kras*$^{G12D/+}$;*Trp53*^{R172H};*p48*-Cre, denoted as *KPC*) (7). The *KPC* model has been predictive of therapeutic responses in patients (reviewed in (8,9)).

Mesothelin (Msln) is a self-antigen that has low expression in mesothelial cells that line vital organs, including the lung and the heart (10), and in fibroblasts during inflammation (11). Msln has high expression in pancreatic tumor cells (6,12), and therapy with TCR_{Msln} $CD8^+$ T cells targets the tumor specifically, without overt toxicities to normal tissues (6). We have also isolated corresponding human TCRs for clinical translation. However, because infused TCR_{Msln} cells in the *KPC* model become progressively dysfunctional in the tumor and contract in number over time, repeated T-cell infusions are administered to achieve therapeutic benefit (6) and strategies to modulate the tumor microenvironment (TME) could enhance potency.

PDAs are notorious for robust desmoplasia, orchestrated largely by activating mutations in the *Kras* proto-oncogene. Myeloid cells, particularly tumor-associated macrophages (TAMs), predominate in the tumor stroma (13–15). TAMs often express immunosuppressive factors and inhibitory ligands, support tumor angiogenesis, and inhibit endogenous T cells (16). Nevertheless, we have found that T cells co-localize with TAMs *in situ* in human PDA, and the presence of T-cell infiltrates correlates positively with TAM numbers (15). Thus, modulating TAMs could potentially be leveraged to enhance T cell-based therapies.

In healthy tissues, macrophage homeostasis is maintained by macrophage colony-stimulating factor (Csf1), which promotes differentiation of hematopoietic stem cells toward the myeloid lineage during development and inflammation (17). Csf1 binds the receptor Csf1R, inducing phosphorylation and activation of several signaling pathways, including Mapk and Stat3, to promote myeloid cell survival and proliferation. Csf1R signaling can also promote immune tolerance to transplantation antigens (18) and Csf1R blockade depletes TAMs and enhances endogenous T-cell antitumor activity in several mouse cancer models (19,20). Targeting this pathway is in early-stage clinical trials and has exhibited antitumor activity in diffuse-type tenosynovial giant cell tumors (21).

Changing the functionality of TAMs in tumors from a suppressive state to an antitumor state (TAM programming) could be a promising alternative to TAM depletion for cancer therapy. Beatty *et. al.*, showed that anti-CD40 can increase recruitment of TAM precursors with direct tumoricidal function into PDA (13). Anti-CD40 did not reprogram suppressive TAMs within the tumor, but instead recruited tumoricidal TAM progenitors. Unexpectedly, the antitumor effects of anti-CD40 were independent of endogenous T cells. Agonistic anti-CD40 also improves response to immune checkpoint blockade in pancreatic cancer models (22), potentially reflecting recruitment and activation by anti-CD40 of $Batf3^{+}$ dendritic cells (DCs) (23).

Here, we investigated the impact of TAM depletion using Csf1R blockade or TAM programming with agonistic anti-CD40 in combination with TCR_{Msln}-engineered cell therapy in *KPC* mice. The results demonstrated that TAM depletion diminished the antitumor activity of infused effector $CD8^{+}$ T cells, whereas TAM programming enhanced the accumulation and longevity of TCR_{Msln}-engineered cells but still failed to overcome engineered T-cell dysfunction in the tumor microenvironment. The results support both the safety and clinical potential of anti-CD40 and engineered T-cell therapy for PDA patient treatment, yet, also highlight the potential for immune modulation that impact endogenous vs. adoptively transferred T cells distinctly, as well as the need for further investigation into fundamental mechanism(s) governing antigen-specific T-cell dysfunction in pancreatic cancer.

MATERIALS & METHODS

Animals

The Fred Hutchinson Cancer Research Center (FHCRC), University of Washington, and the University of Minnesota Institutional Animal Care and Use Committees approved all animal studies. $Kras^{LSL\text{-}G12D/+}$;$Trp53^{LSL\text{-}R172H/+}$;$p48^{Cre}$ (*KPC*) mice (Fred Hutchinson Cancer Research Center) mice initially generated on a mixed background (7) and were serially backcrossed to C57Bl/6J mice (The Jackson Laboratory; Stock No 00664) and determined to be >99.6% pure by SNP analyses as previously described (6). The animals were housed at the Fred Hutchinson Cancer Research Center and University of Minnesota. P14 mice (24), which are of C57Bl/6J origin, were bred to the $Thy1.1^{+}$ congenic strain (The Jackson Laboratory; Stock 000406) to generate P14 $Thy1.1^{+/+}$ or P14 $Thy1.1^{+/-}$ T cells as a source for engineering and housed at the University of Washington and University of Minnesota.

Human pancreatic cancer samples

Surgically resected PDA specimens were obtained from patients (n=11) who provided written informed consent by NWBioTrust (Department of Pathology, University of Washington School of Medicine). PDA samples were selected from patients who underwent surgery without neoadjuvant therapy, and this study cohort has been previously described (15). Resected tumor and normal adjacent (Nadj) pancreas were collected immediately following surgery and placed into ice cold complete media (DMEM containing 10% FBS + 1% Penicillin/Streptomycin). Tissues were subdivided for flash frozen (RNA/DNA) or were further processed to generate single-cell suspensions of mononuclear cells. In the latter case, tumors were weighed, minced with a razor blade, incubated for 30 minutes in collagenase (1 mg/mL), mechanically filtered (70 μM), and washed twice in complete media. Single-cell suspensions were cryopreserved in 10% DMSO and stored at −80°C for subsequent analysis. Tissues for gene expression analyses were flash frozen in liquid nitrogen and stored at −80°C for further processing. All studies using human specimens were approved by the Fred Hutchinson Cancer Research Center Institutional Review Board and conducted according to the principles expressed in the Declaration of Helsinki.

Generation of retroviral vector

A retroviral vector containing the high-affinity mesothelin-specific (1045) TCR was generated as previously described (6). Briefly, 2.2×10^6 Platinum-E (Plat-E, ATCC) retroviral packaging cells were plated on 10 cm tissue culture-treated plates in Plat-E media [DMEM (Gibco), 10% FBS (Gibco), 2% L-glutamine (Sigma), 1% Pen/strep (Sigma), blasticidin(10 μg/mL, Sigma), puromycin(1 μg/mL, Sigma)] for 24 hours at 37°C, 5% CO_2. On day 2, Plat-E cells were transfected with the MIGRI-TCR1045α-P2A-TCR1045β plasmid using Effectene (Qiagen). The MIGRI plasmid has been previously described (25). The cloning of the high-affinity 1045 TCR has been previously described (6). On day 3, Plat-E media was replaced with T-cell media (DMEM, 10% FBS, 2% L-glutamine, 1% Pen/strep, β-mercaptoethanol), and cells were further incubated at 32°C, 5% CO_2. On days 4 and 5, viral supernatants were harvested and passed through a 0.45 μM filter (Sigma) for immediate use.

Generation of TCR_{Msln}-engineered T cells

Single-cell suspensions of mononuclear cells from female P14 $Thy1.1^+$ spleens were generated by mechanical disruption and red blood cell lysis (ACK). Splenic mononuclear cells were stimulated *in vitro* with anti-CD3 (1 μg/mL; clone 145–2C11, BD Biosciences) and anti-CD28 (1 μg/mL; clone 37.51, BD Biosciences) in 10 mL of complete T-cell media containing recombinant human IL2 (rIL2, 50 U/mL) upright in T25 flasks at 37°C, 5% CO_2. On day 1 and day 2 post-stimulation, bulk splenocytes containing activated T cells were transduced with the MIGRI-TCR1045α-P2A-TCR1045β retrovirus by spinfection in 12-well plates containing polybrene (10 μg/mL) and rIL2 (50 U/mL) for 90 minutes at 1000 x *g* at 30°C as described (6). On day 5, T cells were screened for transduction efficiency by flow cytometric staining with CD8-e450 (clone 53–6.7; BD Biosciences), Thy1.1-PerCP (clone OX-7; BD Biosciences), Vβ9-PE (clone MR10–2; BD Biosciences) and/or a $Msln_{406–414}$-H-$2D^b$-APC tetramer generated by the FHCRC Immune monitoring core. On day 7 post *in*

vitro stimulation, transduced T cells were re-stimulated *in vitro* with peptide-pulsed, irradiated splenocytes from B6 mice (3500 R) at a 5:1 APC to T-cell ratio in the presence of rIL2 (50 U/mL). All T-cell cultures were supplemented with rIL2 (50 U/mL) every other day for the duration of *in vitro* culture. On day 5 post the 2nd stimulation *in vitro*, >90% of the $CD8^+Thy1.1^+$ T cells expressed TCR_{MSLN}. T cells were re-suspended in sterile saline and infused into mice as described below.

Adoptive T-cell therapy

We previously described a protocol optimized to promote the expansion of mesothelin TCR-engineered cells in mice (6). Briefly, *KPC* mice are enrolled in treatment studies when they achieve 3–6 mm pancreatic tumors as determined by serial monitoring with high-resolution ultrasound (Vevo 2100). Enrolled mice received cyclophosphamide (Cy, 180 mg/kg, IP, UW Pharmacy), and 6 hours later received IP 1×10^7 congenic ($Thy1.1^+$) $CD8^+$ transduced to express the high-affinity TCR_{Msln} (1045(6)) + 5×10^7 irradiated and peptide ($Msln_{406–414}$, GQKMNAQAI)-pulsed syngeneic splenocytes. Engineered T cells had been stimulated 2X *in vitro* prior to transfer (described above). Recipients also received rIL2 (2×10^4 U/IP every other day for 8 days) to promote T-cell expansion after transfer.

In vivo antibody treatments

KPC mice with 3–6 mm tumors were injected with purified anti-CSF1R (anti-CD115, clone AFS98)(18) derived from a hybridoma generously provided by Dr. Miriam Merad (Icahn School of Medicine at Mount Sinai, New York, NY). Mice received 1 mg/mouse IP on day −3 and day 0 (*e.g.*, day of T-cell therapy), followed by bi-weekly injections of 0.5 mg/mouse IP for 8 or 28 days. A separate cohort of *KPC* mice was treated once with 100 μg agonistic anti-CD40 (FGK145 hybridoma kindly provided by Dr. Stephen Schoenberger, La Jolla Institute for Allergy and Immunology, San Diego, CA) or isotype control (Rat IgG2a, 2A3; Bioxcell). Anti-CSF-1R and anti-CD40 were purified from culture supernatants of hybridomas grown in a CELLine Flask (BD) in serum-free Hybridoma medium (Sigma) or purchased from BioXcell.

Mouse tissue preparation

Peripheral blood mononuclear cells (PBMCs) were collected prior to organ harvest. Blood was collected in PBS containing 20 mM EDTA, then lysed with 1X ACK Lysis buffer (Thermo Fisher) at room temperature and centrifuged at 10,000 rpm for 1 minute. PBMCs were then resuspended in 1 ml complete media (DMEM containing 10% FBS + 1% pen/strep), stored on ice for <2 hours and subsequently stained for flow cytometric analyses. Tumor, pancreas, spleen, metastases, or lung were also collected and placed into ice cold media (DMEM containing 10% FBS + 1% pen/strep). Tissues were subsequently divided for analyses for RNA (flash frozen), immunohistochemistry (formalin-fixed), and immunofluorescence (OCT compound). For flow cytometric analyses of single cells, tissues were weighed, minced, and then incubated for 20 minutes in collagenase (1 mg/mL; Sigma) at 37°C, filtered (70 μm filters, Sigma), and washed 2X in complete media. Live cells were counted by Trypan blue exclusion.

Flow cytometry

Single-cell suspensions of mononuclear cells isolated from blood, spleen, and tumor were stained with the following fluorophore-conjugated monoclonal antibodies: CD45 (Ly5; Biolegend), Thy1.1 (OX-7; BD Biosciences), CD8α (53–6.7; BD Biosciences), CD11b (M1/70; BD Biosciences), Ly6C (HK1.4; Biolegend), Gr-1 (RB6-8C5; BD Biosciences), CD115 (AFS98; Biolegend), PD-1 (J43; ThermoFisher), granzyme B (NGZB; Biolegend), IFNγ (XMG1.2; BD Biosciences), TNFα (MP6-XT22; BD Biosciences), CD11c (N418; Biolegend), CD64 (X54-5/7.1; Biolegend), SIRPa (P84; Biolegend), Ly6G (1A8; Biolegend), CD19 (1D3; BD), and NK1.1 (PK136; eBioscience). Human antibodies used included CD11b (ICRF-44; eBioscience), CD115 (12-3A3-1B10; eBioscience), and CD163 (GH1/61; Biolegend). To measure intracellular cytokine production, engineered T cells ± $Msln_{406–414}$ peptide or gp33 peptide (KAVYNFATM, Genscript) were incubated *in vitro* for 5 hours in the presence of GolgiPlug (5 μg/mL; BD Biosciences), stained for surface antigens, fixed and permeabilized (BD Biosciences Fixation/Permealization kit, according to protocol), and then stained with appropriate antibodies. To quantify frequency of cells expressing intranuclear proteins T-bet (4B10), Foxp3 (FJK-16s), Eomes (Dan11mag), and Ki67 (SolA15), cells were surface stained, as indicated above, followed by eBioscience Foxp3 Fixation/Permeablization solutions prior to nuclear staining. Data were acquired on an LSRII or FacsCanto (BD Biosciences) and analyzed using FlowJo v10.3 software. Cell numbers infiltrating tissues were normalized to tumor or spleen weight.

Gene expression analysis

RNA was generated from flash frozen tumor samples using the Qiagen RNAeasy kit according to the manufacterer's protocol. RNA content was confirmed using a Nanodrop and 100 ng of RNA were used for each reaction. The standard NanoString Technologies hybridization protocol was followed at the Fred Hutchinson Cancer Research Center Genomics facility. Gene expression was determined using the nCounter PanCancer Immune Profiling Panels (both mouse and human specific kits, Nanostring Technologies). Reporter gene-specific nucleic acid probes appended with fluorophore barcodes were detected and used to quantify a specific subset of immune genes (26). The data were quality controlled according to Nanostring's protocols. Gene expression was analyzed using nSolver v4.0 (Nanostring Technologies).

Histology and immunohistochemistry

Tumors were fixed in 10% formalin for 48 hours and paraffin embedded. 4 μm sections were stained with hematoxylin and eosin (H&E), Masson's trichrome, or Picrosirius red at the University of Washington Histology Core. Primary antibodies used recognized CD163 (Novocastra, 10D6, 1:200), cleaved caspase 3 (Cell Signaling, D175, 1:200), and Ki67 (Thermo Fisher, clone SolA15, 1:200). Slides were scanned using the Nanozoomer Digital Pathology slide scanner (Hamamatsu; Bridgewater, New Jersey), and Visiopharm software (Hoersholm, Denmark) was used to identify regions of interest (ROI, i.e. tumor tissue, excluding normal tissue) sampled at 100%. The software was trained to detect immunoreactivity using a project-specific configuration based on a threshold of pixel values as we previously reported (6). The number of positively stained cells was measured in 3–5

non-overlapping 20X fields using NIS-Element imaging software (Nikon's universal software platform, n=3–5 mice per group). Collagen was quantified from 2 tumor sections stained with Picrosirius red, and intensity of the red staining was assessed in a blinded manner across 3–5 20X fields as follows: 0, no staining detected; 1, light staining; 2, moderate; 3, moderate-high staining intensity; 4, high staining, as we previously described (6) (n= 3–6 animals per cohort).

Immunofluorescence

Normal pancreas and tumors were embedded in OCT (Tissue-Tek), frozen, and stored at −80°C. 7 μm sections were fixed in acetone at −20°C for 10 minutes. Sections were rehydrated with PBS + 2.5% bovine serum albumin (BSA) and incubated for 1 hour at room temperature with primary antibodies to CD11b-PE/Dazzle (Biolegend, M1/70; 1:200), CD8α (BD, 53–6.7; 1:25), panCK-FITC (Sigma-Aldrich, F3418; 1:200) diluted in PBS + 2% BSA. Slides were washed three times in PBS + 2.5% BSA and incubated with anti-mouse 546 (1:1000, Invitrogen) for 1 hour at room temperature in the dark to detect $CD8^+$ T cells. Slides were then washed 3X with PBS + 2% BSA, washed 3X with PBS, and mounted in DAPI Prolong Gold (Life Technologies). Images were acquired on a Leica DM6000 epifluorescent microscope at the University of Minnesota Center for Immunology and analyzed using Imaris 9.1.0 (Bitplane).

The Cancer Genome Atlas (TCGA) analysis

Correlation between myeloid gene and cytokines gene expression in Figure 1 are in whole based upon data generated by the TCGA Research Network: https://www.cancer.gov/tcga. The data includes a total of 165 primary pancreatic ductal adenocarcinomas available from TCGA and analyzed using excel and Graphpad software. A large subset of these have been described (27).

Statistical analyses

Statistical analysis were performed using GraphPad software. All mouse experiments reflect n=3–5 mice per group. Student's t-test was used to compare 2-group data. One-way ANOVA and Tukey post-test were used for multiple comparisons. Pearson r was used to determine correlational significance. Data were expressed as mean ± SEM. p <0.05 was considered significant. *, $p < 0.05$; ** $p< 0.005$; ***, $p < 0.0005$.

RESULTS

Tumor-associated macrophages are elevated in human and mouse PDA and express Csf1R

We previously showed a positive correlation between $CD163^+$ macrophage abundance and localization with endogenous $CD8^+$ T cells in human PDA (hPDA), with a fraction of $CD163^+$ macrophages expressing PD-L1 (15). CD163 is often used to identify immunosuppressive, pro-tumorigenic M2 macrophages (28), but it is also expressed by some tissue-resident macrophages including a sub-population of perivascular macrophages in the central nervous system (29). In further analyses of these tissues described in our prior study (15), we found *CSF1* (M-CSF) to be significantly increased in invasive PDA (n=11) compared with normal adjacent pancreas tissue (n=3)(Fig. 1a). In contrast, *CSF2* (GM-CSF)

and *CSF3* (G-CSF) were not significantly different between normal adjacent pancreas and tumors in patient samples. Gene expression analyses in pancreatic tumors in the TCGA database (30) showed a significant correlation between *CD163* and *CSF1* , between *CSF1* and its receptor *CSF1R*, and between *CD163* and *CSF1R* (Fig. 1b). In contrast to CD11b $^{+}$CD163^{-} cells, most of the CD11b^{+}CD163^{+} macrophages in hPDA expressed CSF1R (CD115)(Fig. 1c–d). Consistent with prior studies (13,14), CD11b^{+} myeloid cells were abundant in both pre-invasive lesions (pancreatic intraepithelial neoplasms, PanINs), primary pancreatic tumors, and spontaneous metastases in *KPC* mice (Fig. 1e). *CSF1* was similarily increased in human and mouse PDA relative to normal pancreas tissue, whereas *CSF2* and *CSF3* were significantly higher in mouse compared to human PDA (Fig. 1f). In contrast to normal mouse pancreas, normal adjacent human pancreas is not truely normal, which can contribute to differences when comparing mouse and human gene expression data. Tissue macrophages can be M1-like and express high MHC II, costimulatory molecules and IL12 (13)(in mice, also express high Ly6C and contribute to antitumor responses (31)) or M2-like, which are characterized by low Ly6C and MHC II expression and produce the immunosuppressive cytokine IL10 (32). Granulocytes express high Gr-1 (and Ly6G) and have intermediate expression of Ly6C (Ly6C^{int}), whereas mononuclear phagocytes do not express Ly6G (33). We differentiated between granulocytes (CD45^{+}CD11b^{+}Gr1^{high}Ly6C^{int}), Ly6C^{high} TAMs (CD45^{+}CD11b^{+}Ly6C^{high}), and Ly6C^{low} TAMs (CD45^{+}CD11b^{+}Gr-1^{-}Ly6C^{-})(Fig. 1g). The most frequent intratumoral CD11b^{+} subset in *KPC* mice was Ly6C^{low} TAMs. The phenotypes of cells identified using this gating strategy were further assessed and included CD19^{+} B cells and intratumoral NK cells (NK1.1^{+}) as control cell populations. Both Ly6C^{high} and Ly6C^{low} TAMs expressed common mononuclear myeloid markers CD11c, CD64, and SIRPα and had variable expression of MHC II (Fig. 1h). Csf1R (CD115) expression, albeit dim, was expressed the highest on intratumoral Ly6C^{low} TAMs (Fig. 1h).

Csf1R blockade depletes TAMs and remodels the extracellular matrix in autochthonous PDA

To investigate the direct role of Csf1R signaling on myeloid subsets and indirect impact on antigen-specific T cells, we administered a monoclonal antibody against Csf1R (anti-Csf1R/CD115 (18)) in combination with Msln-speciifc T cells according to a therapy protocol previously shown to have activity in *KPC* mice with invasive disease (6)(Fig. 2a), which includes administration of cyclophosphamide (Cy) to achieve transient lymphodepletion, followed by (6 hours later) infusion of 1×10^{7} P14 Thy1.1^{+} T cells retrovirally transduced to express a high-affinity TCR specific for Msln$_{406–414}$/H-2D^{b}. The transduced T cells were stimulated twice *in vitro* with antigen and expanded in recombinant human IL2 prior to transfer. To promote expansion of transferred engineered T cells, recipient animals also received as a vaccine 1×10^{7} irradiated syngeneic splenocytes pulsed with Msln peptide (6). As seen in healthy animals (34), Csf1R had high expression on circulating Ly6C^{high} inflammatory monocytes (IMs) and Ly6C^{low} patrolling monocytes (PMs) in untreated *KPC* mice (Fig. 2b). At day 8 post T-cell infusion, anti-Csf1R did not significantly modify circulating CD45^{+} or CD11b^{+} cell frequencies, but did significantly reduce both circulating monocyte populations, while concomitantly increasing granulocyte frequency (Fig. 2c). By day 28, PM precursor frequency remained significantly decreased in the blood, whereas IM

frequency rebounded to near baseline levels (Fig. 2c). PMs are relatively long-lived in circulation (>1 week) compared to IMs, which have a circulating half-life <4 hours and rapidly differentiate into PMs in wild-type mice (34). The half-life of IMs in tumor-bearing mice may be slightly prolonged because of myeloid cytokines such as Csf1 secreted by pancreatic tumor cells (14). However, the fact that Csf1R blockade caused sustained reduction of PMs but not IMs, suggests that either Csf1R signaling promotes IM differentiation into PMs or that the kinetics of conversion and/or replenishment of IMs are altered in cancer.

We next investigated whether intratumoral myeloid subsets were altered by Csf1R blockade. At day 8 post T-cell transfer, anti-Csf1R treatment significantly decreased $Ly6C^{low}$ TAM frequency resulting in a 2-log reduction in number (Fig. 2d). As seen with circulating granulocytes, both the frequency and number of intratumoral granulocytes were also significantly increased with Csf1R blockade at day 8 (Fig. 2d), a finding also observed in some transplantable tumor models (35). In contrast with day 8 findings, granulocytes were instead significantly reduced by day 28 after Csf1R blockade (Fig. 2e). $Ly6C^{low}$ TAM frequency remained significantly reduced compared to control tumors 28 days after treatment with engineered T cells and anti-Csf1R (Fig. 2e). Thus, Csf1R blockade had differential temporal effects on intratumoral granulocytes during the treatment course.

Histological analyses were performed to determine if Csf1R blockade and TAM depletion affected the stroma. We previously showed that administration of TCR_{Msln} significantly altered the stroma, as characterized by collagen reduction in the extracellular matrix (ECM), which was evident at day 8 but not sustained to day 28 post-transfer when the T cells have largely lost function (6). However, concomitant Csf1R blockade maintained ECM loss at 28 days post T-cell transfer (Supplementary Fig. S1a-b**)**. Thus, Csf1R signaling may promote ECM deposition and/or stability, potentially by promoting survival and/or proliferation of a subset of fibro-inflammatory TAMs (36,37). Anti-Csf1R treatment significantly decreased tumor apoptosis at both 8 and 28 days following infusion of TCR_{Msln}-engineered T cells (Supplementary Fig. S1c). We also observed a trend for reduced tumor cell proliferation in anti-Csf1R–treated mice compared to controls, suggesting Csf1R signaling may support tumor cell proliferation (Supplementary Fig. S1d). Quantification of collagen showed a significant decrease due to anti-Csf1R treatment (Supplementary Fig. S1e). ECM remodeling may influence tumor cell survival and/or proliferation, as well as have effects on engineered T-cell migration and accumulation.

Csf1R blockade differentially effects endogenous and engineered T cells

We next investigated how Csf1R blockade influenced polyclonal endogenous $CD8^+$ T cells compared to engineered tumor antigen–specific T cells. Anti-Csf1R caused a significant increase in frequencies of both endogenous ($CD8^+Thy1.1^-$) and TCR_{Msln}-engineered ($CD8^+Thy1.1^+$) T cells in both circulation and in tumors of *KPC* mice (Fig. 3a–c). Endogenous $CD8^+$ T-cell number increased 5- to 10-fold in tumors at both early and later time points (Fig. 3d). In contrast, intratumoral engineered T-cell numbers were unchanged at day 8 and only modestly increased (~2-fold) at day 28 (Fig. 3e). Thus, despite significantly lowering the TAM:engineered T-cell ratio by 6 to 8-fold (Fig. 3f) and enhancing

accumulation of endogenous T cells and frequency of engineered T cells, Csf1R blockade had limited impact on engineered T-cell expansion and accumulation. We previously showed that TCR_{Msln}-engineered T cells become progressively dysfunctional in PDA, as characterized by reduction in tumor cell killing and loss of ability to produce IFNγ (6). The addition of Csf1R blockade resulted in a higher frequency of dysfunctional engineered T cells in the tumor at day 8 post-transfer (Fig. 3g–h), which correlated with a higher frequency of cells expressing PD-1 (Fig. 3i).

The unanticipated finding that TAM depletion did not enhance engineered T-cell function in PDA prompted us to quantify the impact of T-cell therapy alone on myeloid cell composition in PDA. Serial (bi-weekly) TCR_{Msln} cell infusions into *KPC* mice modified the frequency and number of intratumoral myeloid subsets. A significant increase in $Ly6C^{high}$ $CD11b^{+}$ frequency and number was observed after treatment with TCR_{Msln} cells but not control T cells (Fig. 3j), and intratumoral $Ly6C^{high}$ $CD11b^{+}$ cell frequency significantly correlated with mouse survival (Fig. 3k). Thus, T-cell therapy promoted the recruitment, survival and/or expansion of $Ly6C^{high}$ TAMs in PDA. Although it remains unclear what factors activated T cells produce to influence the recruitment and/or expansion of myeloid cells, possibilities include CCL2, CCL5, or GM-CSF (38). Additional investigation into the cross-talk between tumor-reactive T cells and myeloid cells in the tumor microenvironment should help improve immunotherapy design.

Anti-CD40 promotes expansion and persistence of TCR_{Msln}-engineered cells in *KPC* mice

Because TAM depletion failed to augment TCR_{Msln} cell function and TCR_{Msln} cell therapy efficacy correlated with TAM accumulation (Fig. 3j), we next tested if modulation of TAM function rather than depletion could enhance engineered T-cell antitumor effects. Agonistic anti-CD40 promotes the influx of monocytes into PDA, which can differentiate into tumoricidal macrophages or dendritic cells (13,23). However, it is not known if anti-CD40 can enhance self/tumor-reactive engineered effector T cells. Therefore, we administered a single dose of anti-CD40 at the time of TCR_{Msln}-engineered cell therapy in *KPC* mice (Fig. 4a). Anti-CD40 dramatically enhanced both the acute expansion and persistence of infused $CD8^{+}Thy1.1^{+}$ TCR_{Msln}-engineered T cells in circulation (Fig. 4b–c). PD-1 on circulating TCR_{Msln} cells was significantly lower in mice that received anti-CD40 compared to isotype control for at least 14 days post-transfer (Fig. 4c), suggesting that anti-CD40 may enhance the quality of infused T cells. Anti-CD40 resulted in >10-fold increase in intratumoral engineered T-cell numbers at day 8 (Fig. 4d) and day 28 (Fig. 4e). Anti-CD40 also significantly increased the frequency and number of infused T cells in the lung at day 8, a site where mesothelin had low expression (Fig. 4d) without evidence of respiratory distress or toxicity to normal tissues, suggesting this may be non-specific (Supplementary Fig. S2). By day 28, the number of infused T cells in the lung was no longer significantly different (Fig. 4e). *In situ* staining showed that anti-CD40 increased $CD8^{+}$ T-cell accumulation in PDA (Fig. 4f). Anti-CD40 also significantly increased the frequency of infused T cells that express Ki67 and/or the cytolytic molecule granzyme B at day 28 (Fig. 4g–i). However, anti-CD40 did not rescue engineered T-cell IFNγ production in PDA (Fig. 4j–k). This was not due to specific deficiencies in the introduced TCR signaling because stimulation of the engineered T cells via the endogenous TCR (P14 which recognizes gp33/H-$2D^{b}$) also did

not rescue function. IFNγ production by splenic TCR_{Msln} cells was significantly diminished after a single dose of anti-CD40 compared to TCR_{Msln} cells isolated from control or isotype treated mice (Fig. 4k), which may reflect changes in the local inflammatory environment in the spleen following anti-CD40. Taken together, these data indicate that anti-CD40 promotes engineered tumor-reactive T-cell longevity but fails to fully rescue function of engineered T cells in pancreatic cancer.

Anti-CD40 with engineered T cells increases tumor cell apoptosis and alters the tumor stroma

Previously we showed that a single infusion of engineered T cells had only transient antitumor activity (6). To test if anti-CD40 prolonged antitumor activity, we assessed stroma remodeling and tumor cell apoptosis. Anti-CD40 sustained collagen loss and tumor cell killing following engineered T-cell infusion through day 28 post-infusion (Fig. 5a–c). Histological analyses of the heart and lung, sites of normal mesothelin expression, showed no evidence of increased apoptosis or pathological damage (Supplementary Fig. S2**)**. To gain insight into how anti-CD40 might promote T-cell persistence and tumor cell killing, we evaluated the immune composition in the tumors following treatment. Anti-CD40 in combination with TCR_{Msln} T cells significantly increased the frequency of both $CD45^+$ hematopoietic cells (Fig. 5d) and $CD11b^+$ myeloid cells (Fig. 5e) at day 8. Anti-CD40 plus T-cell therapy increased granulocyte frequency at day 8 but decreased it by day 28 (Fig. 5d). Anti-CD40 also significantly increased the frequency and number of $Ly6C^{high}$ TAMs in PDA at day 8 post T-cell transfer (Fig. 5d–e), while leaving the number of $Ly6C^{low}$ TAMs unchanged. PD-1, an inhibitory receptor that has been identified on immunosuppressive M2-like TAMs that interfere with tumor immunity (39), was highly expressed on the $Ly6C^{low}$ TAMs (Fig. 5f). However, anti-CD40 reduced the frequency of these $PD\text{-}1^+Ly6C^{low}$ TAMs with a corresponding increase in $Ly6C^{high}PD\text{-}1^{low}$ TAM at day 8 (Fig. 5f). Taken together, these data support potential benefits of myeloid programming rather than ablation to enhance antitumor activity of engineered T-cell therapy, and is supported by the fact that *CSF1* expression trends with prolonged PDA patient overall survival (Supplementary Fig. S3). However, there are clearly additional barriers that suppress sustained engineered T-cell cytokine production that are not overcome by these specific myeloid-targeted therapies. The enhanced tumor killing may reflect the activity of anti-CD40 in promoting tumoricidal macrophages, as has been reported in PDA (13). The cyclophosphamide preconditioning regimen prior to T-cell therapy transiently induced death of all circulating myeloid cell subsets (Supplementary Fig. S4a-b), which may indirectly impact how myeloid-targeted therapies influence engineered T-cell responses. The results highlight the complexity of activities by myeloid subsets and suggest that the most effective strategies for enhancing adoptive cellular therapies involving transfer of activated effector T cells may differ from the requirements for amplifying evolving endogenous T-cell responses.

DISCUSSION

Most PDA patients succumb rapidly to their disease because of resistance to even the most aggressive therapies. Because current immunotherapies such as anti–PD-1/PD-L1 or anti–CTLA-4 provide minimal therapeutic benefit for the majority of patients, we were pursuing

an engineered T-cell therapy that redirects T-cell specificity to target a commonly overexpressed self/tumor antigen mesothelin (40). Despite significant antitumor activity of these TCR_{Msln} cells in autochthonous murine PDA, intratumoral engineered T cells decrease in both quantity and quality over a relatively short time period (6), suggesting the tumor microenvironment may limit treatment efficacy. TAMs are abundant in mouse and human PDA and are immunosuppressive to endogenous T cells (13,14,36,41). Nevertheless, we found that TAM depletion, including the most abundant $Ly6C^{low}$ subset, following Csf1R blockade had unfavorable effects on engineered T cells. Alternatively, anti-CD40, which increased $Ly6C^{high}$ TAM accumulation without altering $Ly6C^{low}$ TAM numbers and increased the longevity of engineered T cells. However, the changes in TAMs and the myeloid infiltrate in PDA by anti-CD40 were insufficient to maintain the functions of persisting engineered T cells, including cytokine production.

Genetic fate mapping studies have demonstrated that macrophages in most adult tissues arise from yolk-sac derived hematopoietic progenitors during embryonic development (42). Such tissue-resident macrophages perpetuate indefinitely throughout adulthood via stromal cell production of Csf1 that promotes macrophage survival and proliferation (42). In settings of inflammation, such as cancer (43) or atherosclerosis (44), circulating monocytes are recruited into the tissue parenchyma and differentiate into macrophages, contributing to the overall tissue macrophage pool. It has been suggested that Csf1-dependent tissue-resident TAMs form the primary macrophage subset that contributes to PDA growth (36). Our study corroborates previous work demonstrating Csf1R-dependent maintenance of $Ly6C^{low}$ TAMs in PDA (36). These tissue-resident TAMs are a major source of ECM components and angiogenic factors (36). Our observation that $Ly6C^{low}$ TAM depletion following Csf1R blockade decreased collagen and tumor cell proliferation are consistent with tissue-resident TAMs promoting tumor growth, perhaps indirectly by depositing ECM and/or directly via production of factors that can induce EGF/MAPK signaling in tumor cells (37,45).

Our findings suggest that tissue-resident TAMs have differential effects on engineered vs. endogenous T cells. Ablation of $Ly6C^{low}$ TAMs using Csf1R blockade was not sufficient to enhance acute intratumoral accumulation of infused engineered effector T cells, despite increasing endogenous $CD8^+$ T-cell accumulation. Similarly, Csf1R blockade has been shown to deplete the normal pancreas of resident macrophages and prevent diabetes onset mediated by the adoptive transfer of T cells specific to islet antigens (46). By contrast, the impact on accumulation of endogenous T cells is consistent with a study that showed $Ly6C^{low}$ TAMs inhibit endogenous T-cell infiltration and/or prevent their retention in PDA (20). The antigen specificity of such endogenous CD8 T cells is unknown, however, and the enhanced infiltration might be largely non-specific. In contrast to naive or quiescent memory T cells, engineered T cells are activated and differentiated effector T cells that express a distinct set of adhesion molecules and chemokine receptors. Thus, it is possible $Ly6C^{low}$ TAM depletion enhances the expression of chemokines or factors that support endogenous naïve/memory T-cell recruitment, but that such factors are irrelevant for effector T-cell recruitment. Alternatively, the influx of endogenous $CD8^+$ T cells may successfully compete for critical homeostatic cytokines at the tumor site that would otherwise be available for engineered T cells.

The fact that *CSF1* expression trended with prolonged overall survival in pancreatic cancer patients and that TAMs correlated with $CD8^+$ T-cell number and location in human PDA (15) suggest a TAM subset, or specific TAM qualities, in PDA may support effector T-cell responses. Because both tissue resident– and monocyte-derived TAMs can take up tumor antigens (36), MHC I-restricted antigen presentation by TAMs may be critical for sustaining effector functions of engineered T cells. iNOS production by TAMs promote adoptively transferred $CD8^+$ T-cell antitumor activity in a mouse syngeneic lymphoma model (47), whereas iNOS production suppresses naive T-cell activation (48), suggesting loss of iNOS production might preferentially interfere with activity of the infused effector cells.

In contrast to $Ly6C^{low}$ TAM depletion, a single dose of agonistic anti-CD40 enhanced the expansion, intratumoral accumulation, and persistence of adoptively transferred TCR-engineered T cells. CD40, a TNFR superfamily member, has broad cell distribution including macrophages, dendritic cells, B cells, and endothelial cells. In the current report, we focused on the effects of agonistic anti-CD40 on TAMs, which has been identifed as a target (13). Agonistic anti-CD40 can promote upregulation of adhesion molecules on endothelial cells and macrophage proinflammatory cytokine production, which could enhance the accumulation and activation of adoptively transferred tumor antigen-specific $CD8^+$ T cells. Because we observed that infusion of TCR_{Msln} cells increased the accumulation of a similar $Ly6C^{high}$ TAM population without anti-CD40, our data suggest that one potential mechanism of antitumor activity by engineered T-cell therapy is via engaging the myeloid lineage. Thus, the significant increase in tumor cell apoptosis we observed in mice treated with anti-CD40 and TCR_{Msln} cells could in part reflect further enhancement of tumoricidal macrophages, as reported (13).

Combinatorial targeting of TAMs is a potential therapeutic strategy. However, agonistic anti-CD40 administered <3 days prior to chemotherapy has been shown to induce lethal hepatotoxicity in mice via Csf1R-dependent macrophages (49), indicating a sensitivity to timing and sequencing when incorporating multiple treatment modalities. Therefore, given the inherent complexity of our treatment protocol, which includes cyclophosphamide preconditioning, tumor antigen-specific $CD8^+$ T cells, a vaccine, and exogenous IL2 (6), we focused on either Csf1R blockade or an anti-CD40 agonist in combination with T-cell therapy. In mouse immunogenic implantable tumor models, the combination of anti-CD40 and Csf1R blockade synergize to significantly slow tumor growth, whereas Csf1R blockade had no antitumor effect alone (50,51). Using a potentially less immunogenic and genetically engineered melanoma model, similar synergistic antitumor effects of dual anti-CD40 and Csf1R blockade was shown (52). However, these studies required frequent, prolonged, and high dosing of both anti-CD40 and Csf1R blockade. Our results demonstrated no benefit to persistence or function of transferred TCR_{Msln} T cells with Csf1R blockade and anti-CD40 failed to rescue T-cell cytokine production. Our T-cell therapy protocol employs cyclophosphamide preconditioning, which transiently diminishes circulating hematopoietic cells (including all myeloid cell subsets) in the blood, and we did not pursue experiments combining Csf1R blockade and agonist anti-CD40. Because both TAM modulating strategies failed to rescued IFNγ production by engineered T cells in the tumor, future studies will need to elucidate how best to design combinatorial regimens modulating the myeloid compartment with engineered T cells to mazimize therapeutic benefit and minimize

toxicity. Based on our observation of differential responses by engineered T cells compared to endogenous T cells following TAM depletion, studies examining the impact of immune modulating reagents on endogenous anti-cancer immune responses appear insufficient for predicting appropriate combinations for enhancing engineered T-cell therapies.

Supplementary Material

Refer to Web version on PubMed Central for supplementary material.

ACKNOWLEDGEMENTS

I.M.S. is supported by an AACR Pancreatic Cancer Action Network Career Development Award (17-20-25-STRO) and an Institutional Research Grant 124166-IRG-58-001-55-IRG65 from the American Cancer Society. Support was provided by the National Cancer Institute, CA018029 and CA033084 (P.D.G.) and CA161112 (S.R.H.), Giles W. and Elise G. Mead Foundation (to S.R.H.), a Cancer Center Support Grant P30CA015704 Supplement (S.R.H. and P.D.G.) and a Pancreatic Cancer Action Network Grant 16-65-GREE (P.D.G.). P.D.G. receives support from Juno Therapeutics, a Celgene company.

REFERENCES

1. Rahib L, Smith BD, Aizenberg R, Rosenzweig AB, Fleshman JM, Matrisian LM. Projecting cancer incidence and deaths to 2030: the unexpected burden of thyroid, liver, and pancreas cancers in the United States. Cancer Res 2014;74(11):2913–21 doi 10.1158/0008-5472.CAN-14-0155. [PubMed: 24840647]
2. Chiaravalli M, Reni M, O'Reilly EM. Pancreatic ductal adenocarcinoma: State-of-the-art 2017 and new therapeutic strategies. Cancer Treat Rev 2017;60:32–43 doi 10.1016/j.ctrv.2017.08.007. [PubMed: 28869888]
3. Royal RE, Levy C, Turner K, Mathur A, Hughes M, Kammula US, et al. Phase 2 trial of single agent Ipilimumab (anti-CTLA-4) for locally advanced or metastatic pancreatic adenocarcinoma. J Immunother 2010;33(8):828–33 doi 10.1097/CJI.0b013e3181eec14c. [PubMed: 20842054]
4. Brahmer JR, Tykodi SS, Chow LQ, Hwu WJ, Topalian SL, Hwu P, et al. Safety and activity of anti-PD-L1 antibody in patients with advanced cancer. N Engl J Med 2012;366(26):2455–65 doi 10.1056/NEJMoa1200694. [PubMed: 22658128]
5. Lawrence MS, Stojanov P, Polak P, Kryukov GV, Cibulskis K, Sivachenko A, et al. Mutational heterogeneity in cancer and the search for new cancer-associated genes. Nature 2013;499(7457): 214–8 doi 10.1038/nature12213. [PubMed: 23770567]
6. Stromnes IM, Schmitt TM, Hulbert A, Brockenbrough JS, Nguyen H, Cuevas C, et al. T Cells Engineered against a Native Antigen Can Surmount Immunologic and Physical Barriers to Treat Pancreatic Ductal Adenocarcinoma. Cancer Cell 2015;28(5):638–52 doi 10.1016/j.ccell. 2015.09.022. [PubMed: 26525103]
7. Hingorani SR, Wang L, Multani AS, Combs C, Deramaudt TB, Hruban RH, et al. Trp53R172H and KrasG12D cooperate to promote chromosomal instability and widely metastatic pancreatic ductal adenocarcinoma in mice. Cancer Cell 2005;7(5):469–83 doi S1535-6108(05)00128-5[pii]10.1016/ j.ccr.2005.04.023. [PubMed: 15894267]
8. Feig C, Gopinathan A, Neesse A, Chan DS, Cook N, Tuveson DA. The pancreas cancer microenvironment. Clin Cancer Res 2012;18(16):4266–76 doi 10.1158/1078-0432.CCR-11-3114. [PubMed: 22896693]
9. Stromnes IM, DelGiorno KE, Greenberg PD, Hingorani SR. Stromal reengineering to treat pancreas cancer. Carcinogenesis 2014;35(7):1451–60 doi 10.1093/carcin/bgu115. [PubMed: 24908682]
10. Chang K, Pastan I. Molecular cloning of mesothelin, a differentiation antigen present on mesothelium, mesotheliomas, and ovarian cancers. Proc Natl Acad Sci U S A 1996;93(1):136–40. [PubMed: 8552591]

11. Koyama Y, Wang P, Liang S, Iwaisako K, Liu X, Xu J, et al. Mesothelin/mucin 16 signaling in activated portal fibroblasts regulates cholestatic liver fibrosis. J Clin Invest 2017;127(4):1254–70 doi 10.1172/JCI88845. [PubMed: 28287406]
12. Argani P, Iacobuzio-Donahue C, Ryu B, Rosty C, Goggins M, Wilentz RE, et al. Mesothelin is overexpressed in the vast majority of ductal adenocarcinomas of the pancreas: identification of a new pancreatic cancer marker by serial analysis of gene expression (SAGE). Clin Cancer Res 2001;7(12):3862–8. [PubMed: 11751476]
13. Beatty GL, Chiorean EG, Fishman MP, Saboury B, Teitelbaum UR, Sun W, et al. CD40 agonists alter tumor stroma and show efficacy against pancreatic carcinoma in mice and humans. Science 2011;331(6024):1612–6 doi 10.1126/science.1198443. [PubMed: 21436454]
14. Stromnes IM, Brockenbrough JS, Izeradjene K, Carlson MA, Cuevas C, Simmons RM, et al. Targeted depletion of an MDSC subset unmasks pancreatic ductal adenocarcinoma to adaptive immunity. Gut 2014;63(11):1769–81 doi 10.1136/gutjnl-2013-306271. [PubMed: 24555999]
15. Stromnes IM, Hulbert A, Pierce RH, Greenberg PD, Hingorani SR. T-cell Localization, Activation, and Clonal Expansion in Human Pancreatic Ductal Adenocarcinoma. Cancer immunology research 2017 doi 10.1158/2326-6066.CIR-16-0322.
16. Mantovani A, Marchesi F, Malesci A, Laghi L, Allavena P. Tumour-associated macrophages as treatment targets in oncology. Nature reviews Clinical oncology 2017;14(7):399–416 doi 10.1038/nrclinonc.2016.217.
17. Auffray C, Sieweke MH, Geissmann F. Blood monocytes: development, heterogeneity, and relationship with dendritic cells. Annu Rev Immunol 2009;27:669–92 doi 10.1146/annurev.immunol.021908.132557. [PubMed: 19132917]
18. Hashimoto D, Chow A, Greter M, Saenger Y, Kwan WH, Leboeuf M, et al. Pretransplant CSF-1 therapy expands recipient macrophages and ameliorates GVHD after allogeneic hematopoietic cell transplantation. J Exp Med 2011;208(5):1069–82 doi 10.1084/jem.20101709. [PubMed: 21536742]
19. Strachan DC, Ruffell B, Oei Y, Bissell MJ, Coussens LM, Pryer N, et al. CSF1R inhibition delays cervical and mammary tumor growth in murine models by attenuating the turnover of tumor-associated macrophages and enhancing infiltration by CD8 T cells. Oncoimmunology 2013;2(12):e26968 doi 10.4161/onci.26968. [PubMed: 24498562]
20. Zhu Y, Knolhoff BL, Meyer MA, Nywening TM, West BL, Luo J, et al. CSF1/CSF1R blockade reprograms tumor-infiltrating macrophages and improves response to T-cell checkpoint immunotherapy in pancreatic cancer models. Cancer Res 2014;74(18):5057–69 doi 10.1158/0008-5472.CAN-13-3723. [PubMed: 25082815]
21. Cassier PA, Italiano A, Gomez-Roca CA, Le Tourneau C, Toulmonde M, Cannarile MA, et al. CSF1R inhibition with emactuzumab in locally advanced diffuse-type tenosynovial giant cell tumours of the soft tissue: a dose-escalation and dose-expansion phase 1 study. Lancet Oncol 2015;16(8):949–56 doi 10.1016/S1470-2045(15)00132-1. [PubMed: 26179200]
22. Winograd R, Byrne KT, Evans RA, Odorizzi PM, Meyer AR, Bajor DL, et al. Induction of T cell immunity overcomes complete resistance to PD-1 and CTLA-4 blockade and improves survival in pancreatic carcinoma. Cancer immunology research 2015 doi 10.1158/2326-6066.CIR-14-0215.
23. Byrne KT, Vonderheide RH. CD40 Stimulation Obviates Innate Sensors and Drives T Cell Immunity in Cancer. Cell Rep 2016;15(12):2719–32 doi 10.1016/j.celrep.2016.05.058. [PubMed: 27292635]
24. Pircher H, Burki K, Lang R, Hengartner H, Zinkernagel RM. Tolerance induction in double specific T-cell receptor transgenic mice varies with antigen. Nature 1989;342(6249):559–61 doi 10.1038/342559a0. [PubMed: 2573841]
25. Pui JC, Allman D, Xu L, DeRocco S, Karnell FG, Bakkour S, et al. Notch1 expression in early lymphopoiesis influences B versus T lineage determination. Immunity 1999;11(3):299–308. [PubMed: 10514008]
26. Cesano A nCounter((R)) PanCancer Immune Profiling Panel (NanoString Technologies, Inc., Seattle, WA). Journal for immunotherapy of cancer 2015;3:42 doi 10.1186/s40425-015-0088-7. [PubMed: 26674611]

27. Cancer Genome Atlas Research Network. Electronic address aadhe, Cancer Genome Atlas Research N. Integrated Genomic Characterization of Pancreatic Ductal Adenocarcinoma. Cancer Cell 2017;32(2):185–203 e13 doi 10.1016/j.ccell.2017.07.007. [PubMed: 28810144]
28. Hu JM, Liu K, Liu JH, Jiang XL, Wang XL, Chen YZ, et al. CD163 as a marker of M2 macrophage, contribute to predicte aggressiveness and prognosis of Kazakh esophageal squamous cell carcinoma. Oncotarget 2017;8(13):21526–38 doi 10.18632/oncotarget.15630. [PubMed: 28423526]
29. Fabriek BO, Van Haastert ES, Galea I, Polfliet MM, Dopp ED, Van Den Heuvel MM, et al. CD163-positive perivascular macrophages in the human CNS express molecules for antigen recognition and presentation. Glia 2005;51(4):297–305 doi 10.1002/glia.20208. [PubMed: 15846794]
30. Cancer Genome Atlas Research N, Weinstein JN, Collisson EA, Mills GB, Shaw KR, Ozenberger BA, et al. The Cancer Genome Atlas Pan-Cancer analysis project. Nat Genet 2013;45(10):1113–20 doi 10.1038/ng.2764. [PubMed: 24071849]
31. Swirski FK, Wildgruber M, Ueno T, Figueiredo JL, Panizzi P, Iwamoto Y, et al. Myeloperoxidase-rich Ly-6C+ myeloid cells infiltrate allografts and contribute to an imaging signature of organ rejection in mice. J Clin Invest 2010;120(7):2627–34 doi 10.1172/JCI42304. [PubMed: 20577051]
32. Conde P, Rodriguez M, van der Touw W, Jimenez A, Burns M, Miller J, et al. DC-SIGN(+) Macrophages Control the Induction of Transplantation Tolerance. Immunity 2015;42(6):1143–58 doi 10.1016/j.immuni.2015.05.009. [PubMed: 26070485]
33. Stromnes IM, Greenberg PD, Hingorani SR. Molecular pathways: myeloid complicity in cancer. Clin Cancer Res 2014;20(20):5157–70 doi 10.1158/1078-0432.CCR-13-0866. [PubMed: 25047706]
34. Tacke F, Ginhoux F, Jakubzick C, van Rooijen N, Merad M, Randolph GJ. Immature monocytes acquire antigens from other cells in the bone marrow and present them to T cells after maturing in the periphery. J Exp Med 2006;203(3):583–97 doi 10.1084/jem.20052119. [PubMed: 16492803]
35. Kumar V, Donthireddy L, Marvel D, Condamine T, Wang F, Lavilla-Alonso S, et al. Cancer-Associated Fibroblasts Neutralize the Anti-tumor Effect of CSF1 Receptor Blockade by Inducing PMN-MDSC Infiltration of Tumors. Cancer Cell 2017;32(5):654–68 e5 doi 10.1016/j.ccell.2017.10.005. [PubMed: 29136508]
36. Zhu Y, Herndon JM, Sojka DK, Kim KW, Knolhoff BL, Zuo C, et al. Tissue-Resident Macrophages in Pancreatic Ductal Adenocarcinoma Originate from Embryonic Hematopoiesis and Promote Tumor Progression. Immunity 2017;47(3):597 doi 10.1016/j.immuni.2017.08.018. [PubMed: 28930665]
37. Candido JB, Morton JP, Bailey P, Campbell AD, Karim SA, Jamieson T, et al. CSF1R(+) Macrophages Sustain Pancreatic Tumor Growth through T Cell Suppression and Maintenance of Key Gene Programs that Define the Squamous Subtype. Cell Rep 2018;23(5):1448–60 doi 10.1016/j.celrep.2018.03.131. [PubMed: 29719257]
38. Griffith JW, Sokol CL, Luster AD. Chemokines and chemokine receptors: positioning cells for host defense and immunity. Annu Rev Immunol 2014;32:659–702 doi 10.1146/annurev-immunol-032713-120145. [PubMed: 24655300]
39. Gordon SR, Maute RL, Dulken BW, Hutter G, George BM, McCracken MN, et al. PD-1 expression by tumour-associated macrophages inhibits phagocytosis and tumour immunity. Nature 2017;545(7655):495–9 doi 10.1038/nature22396. [PubMed: 28514441]
40. Stromnes IM, Schmitt TM, Chapuis AG, Hingorani SR, Greenberg PD. Re-adapting T cells for cancer therapy: from mouse models to clinical trials. Immunol Rev 2014;257(1):145–64 doi 10.1111/imr.12141. [PubMed: 24329795]
41. Long KB, Gladney WL, Tooker GM, Graham K, Fraietta JA, Beatty GL. IFNgamma and CCL2 Cooperate to Redirect Tumor-Infiltrating Monocytes to Degrade Fibrosis and Enhance Chemotherapy Efficacy in Pancreatic Carcinoma. Cancer discovery 2016;6(4):400–13 doi 10.1158/2159-8290.CD-15-1032. [PubMed: 26896096]
42. Hashimoto D, Chow A, Noizat C, Teo P, Beasley MB, Leboeuf M, et al. Tissue-resident macrophages self-maintain locally throughout adult life with minimal contribution from circulating monocytes. Immunity 2013;38(4):792–804 doi 10.1016/j.immuni.2013.04.004. [PubMed: 23601688]

43. Williams CB, Yeh ES, Soloff AC. Tumor-associated macrophages: unwitting accomplices in breast cancer malignancy. NPJ Breast Cancer 2016;2 doi 10.1038/npjbcancer.2015.25.
44. Tabas I, Lichtman AH. Monocyte-Macrophages and T Cells in Atherosclerosis. Immunity 2017;47(4):621–34 doi 10.1016/j.immuni.2017.09.008. [PubMed: 29045897]
45. Zhang Y, Yan W, Mathew E, Kane KT, Brannon A, Adoumie M, et al. Epithelial-Myeloid cell crosstalk regulates acinar cell plasticity and pancreatic remodeling in mice. Elife 2017;6 doi 10.7554/eLife.27388.
46. Carrero JA, McCarthy DP, Ferris ST, Wan X, Hu H, Zinselmeyer BH, et al. Resident macrophages of pancreatic islets have a seminal role in the initiation of autoimmune diabetes of NOD mice. Proc Natl Acad Sci U S A 2017;114(48):E10418–E27 doi 10.1073/pnas.1713543114. [PubMed: 29133420]
47. Marigo I, Zilio S, Desantis G, Mlecnik B, Agnellini AH, Ugel S, et al. T Cell Cancer Therapy Requires CD40-CD40L Activation of Tumor Necrosis Factor and Inducible Nitric-Oxide-Synthase-Producing Dendritic Cells. Cancer Cell 2016;30(4):651 doi 10.1016/j.ccell.2016.09.009. [PubMed: 27728809]
48. Gabrilovich DI, Ostrand-Rosenberg S, Bronte V. Coordinated regulation of myeloid cells by tumours. Nat Rev Immunol 2012;12(4):253–68 doi 10.1038/nri3175. [PubMed: 22437938]
49. Byrne KT, Leisenring NH, Bajor DL, Vonderheide RH. CSF-1R-Dependent Lethal Hepatotoxicity When Agonistic CD40 Antibody Is Given before but Not after Chemotherapy. J Immunol 2016;197(1):179–87 doi 10.4049/jimmunol.1600146. [PubMed: 27217585]
50. Wiehagen KR, Girgis NM, Yamada DH, Smith AA, Chan SR, Grewal IS, et al. Combination of CD40 Agonism and CSF-1R Blockade Reconditions Tumor-Associated Macrophages and Drives Potent Antitumor Immunity. Cancer immunology research 2017;5(12):1109–21 doi 10.1158/2326-6066.CIR-17-0258.
51. Hoves S, Ooi CH, Wolter C, Sade H, Bissinger S, Schmittnaegel M, et al. Rapid activation of tumor-associated macrophages boosts preexisting tumor immunity. J Exp Med 2018;215(3):859–76 doi 10.1084/jem.20171440. [PubMed: 29436396]
52. Perry CJ, Munoz-Rojas AR, Meeth KM, Kellman LN, Amezquita RA, Thakral D, et al. Myeloid-targeted immunotherapies act in synergy to induce inflammation and antitumor immunity. J Exp Med 2018;215(3):877–93 doi 10.1084/jem.20171435. [PubMed: 29436395]

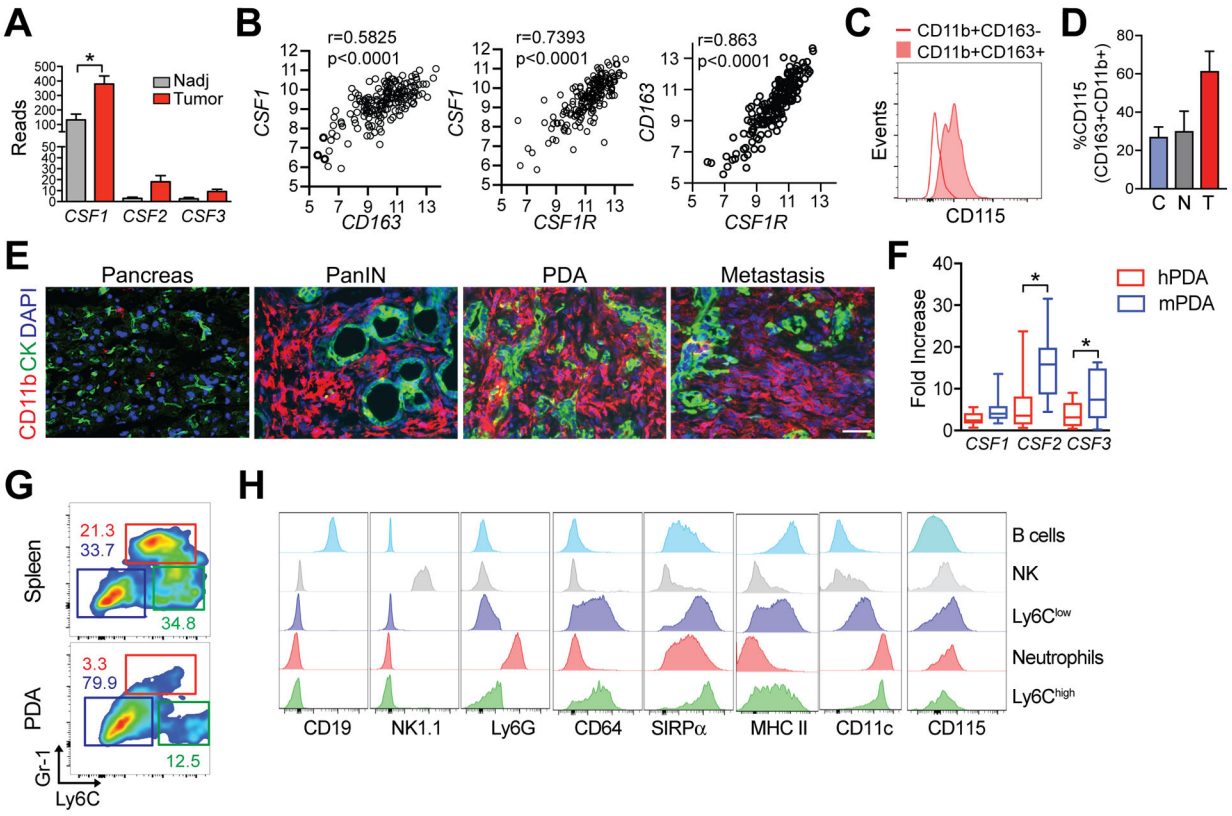

Figure 1. Macrophages are increased in pancreatic cancer and express Csf1R.

a) Expression of *CSF1*, *CSF2*, and *CSF3* in resected human PDA (n=11) and normal adjacent pancreas (Nadj, n=3). Data are mean ± SEM. PanCancer Immune Profiling (Nanostring) was performed once. **b**) Correlations between expression *CSF1, CSF1R*, and *CD163* in human PDA was obtained from TCGA (n=165 samples). **c**) Flow cytometric staining of CD115 on $CD11b^{+}CD163^{+}$ and $CD11b^{+}CD163^{-}$ myeloid cells isolated from resected human PDA. Representative of n=4 independent patient samples. **d**) Frequency of $CD115^{+}$ cells among $CD11b^{+}CD163^{+}$ in circulation (n=3) denoted as C, normal adjacent pancreas (n=2) denoted as N, and tumors (n=4) denoted as T from patients described in (15). **e**) $CD11b^{+}$ (myeloid) and CK^{+} tumor cell staining in *KPC* pancreatic intraepithelial neoplasms (PanIN), primary tumors (PDA), and a diaphragm metastasis. Scale bar, 25 μm. **f**) Fold-increase in gene expression in human PDA (hPDA) vs. mouse PDA (mPDA) determined by comparison to gene expression in normal adjacent pancreas (hPDA) or normal pancreas from wild-type mice (mPDA). **g**) Frequency of granulocytes (red box, $CD11b^{+}Gr1^{high}Ly6C^{int}$), $Ly6C^{high}$ TAMs (green box, $CD11b^{+}Gr1^{int}Ly6C^{high}$), and $Ly6C^{low}$ TAMs (blue box, $CD11b^{+}Gr1^{-}Ly6C^{-}$) in spleen and tumor isolated from a representative *KPC* mouse. Plots are gated on $CD45^{+}CD11b^{+}$ cells. Data are representative of >10 *KPC* tumors analyzed in a similar manner. **h**) Expression of the indicated markers on gated $CD19^{+}$ B cells, NK cells, $Ly6C^{low}$ TAMs, granuolyctes, and $Ly6C^{high}$ TAMs. *, $p<0.05$ as determined by two-tailed unpaired Student's *t* test. Data are representative of n=3 tumors.

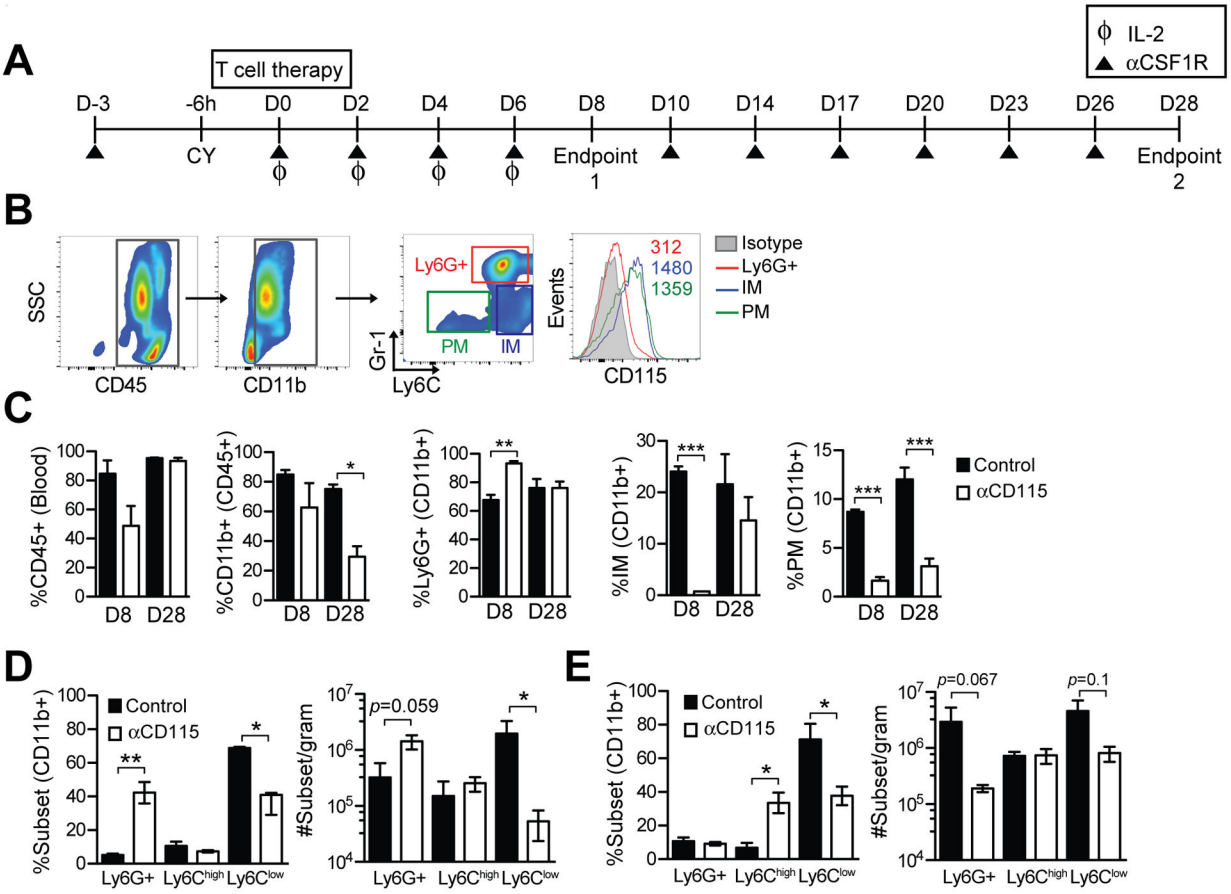

Figure 2. Impact of Csf1R blockade on circulating and intratumoral myeloid cells during adoptive T-cell therapy in PDA.

a) Schematic outlining the treatment of *KPC* mice with TCR_{Msln} T cells ± anti-Csf1R (αCsf1R) or isotype. *KPC* mice received anti-CD115 (anti-Csf1R) at day –3 and at day 0, received cyclophosphamide (CY) followed 6 hours later by engineered TCR_{Msln} T cells plus irradiated peptide-pulsed splenocytes and 6 days of recombinant human IL2. Data represent n=3–4 mice/group and 2 independent experiments. **b**) Gating schematic based on Gr-1 and Ly6C expression to identify circulating myeloid cell subsets: $Ly6G^+$ neutrophils; IMs (inflammatory monocytes); PMs (patrolling monocytes), and Csf1R expression in these populations (histogram). **c**) Frequency of circulating $CD45^+$ cells, $CD11b^+$ cells ($CD45^+$ gate), $Gr\text{-}1^{high}$ ($Ly6G^+$) granulocytes ($CD11b^+$ gate), IMs ($CD11b^+$ gate), and PMs ($CD11b^+$ gate) 8 and 28 days following treatment. Data are mean ± SEM. **d**) Frequency (left graph) of intratumoral myeloid subsets at 8 days post T-cell transfer as determined by gating on $CD45^+CD11b^+$ cells. Number (right graph) of myeloid cell subsets normalized to gram of tissue at day 8. Data are mean ± SEM. **e**) Intratumoral myeloid subset frequency (left graph) at 28 days post T-cell transfer as determined by flow cytometric analyses of $CD45^+CD11b^+$ cells. Myeloid cell number (right graph) normalized to gram of tissue at day 28. Data are mean ± SEM. *, $p<0.05$; **, $p<0.005$; and ***, $p<0.0001$ as determined by two-tailed unpaired Student's *t* test.

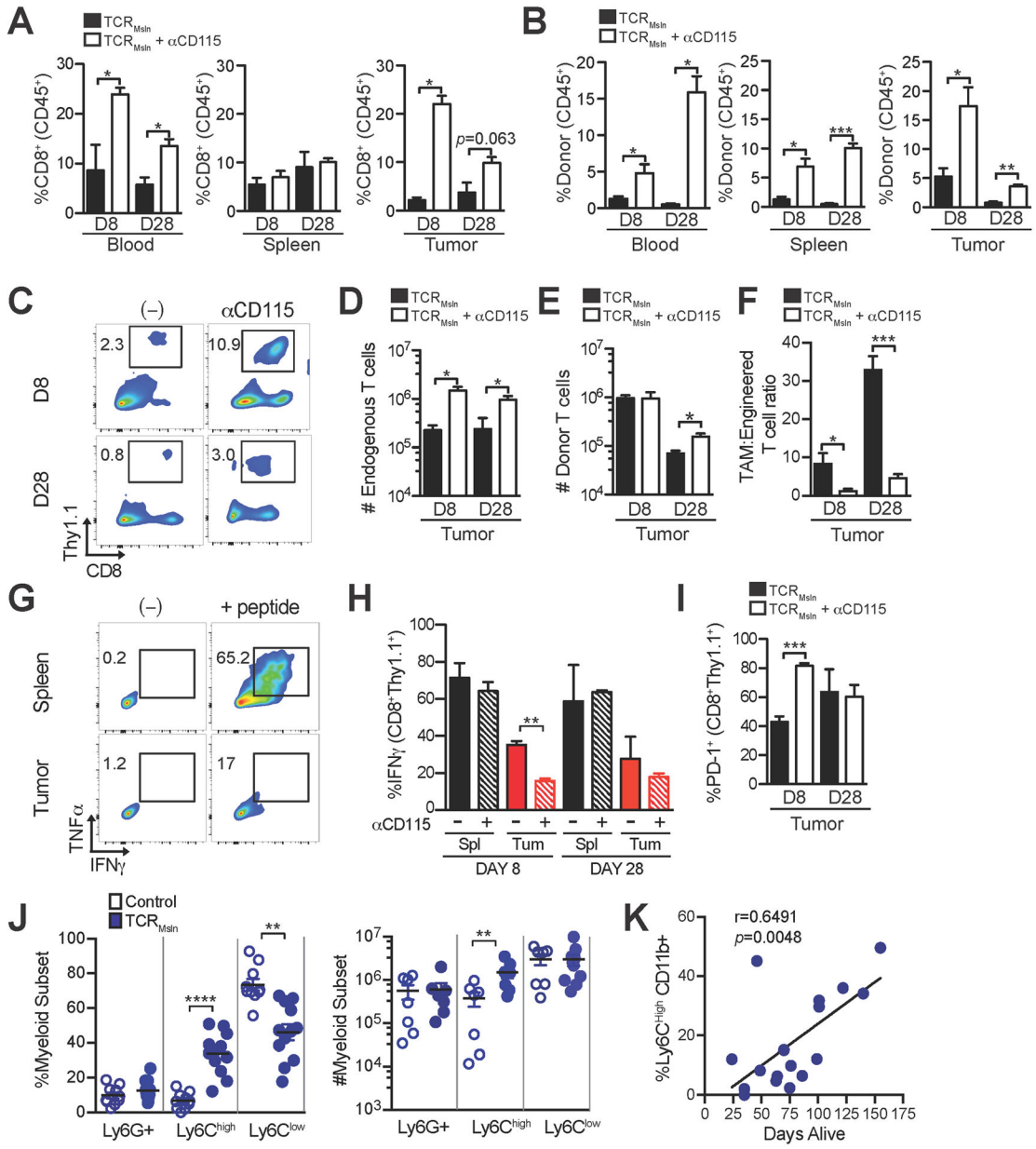

Figure 3. Csf1R blockade differentially influences endogenous and engineered CD8$^+$ T cells.

a) Frequency of endogenous CD8$^+$Thy1.1$^-$ and **b)** engineered CD8$^+$Thy1.1$^+$ T cells in blood and tumor following infusion of TCR$_{Msln}$-engineered T cells ± anti-Csf1R. Percentage of CD8$^+$ T cells was determined by gating on CD45$^+$ cells. **c**) Representative flow cytometric plots of TCR$_{Msln}$ T cells isolated from *KPC* tumors at days 8 and 28 after infusion. Numbers represent the frequency of engineered (CD8$^+$Thy1.1$^+$) TCR$_{Msln}$ cells in PDA of live CD45$^+$ T cells. **d)** Number of endogenous or **e)** donor CD8$^+$ T cells per gram tumor at days 8 and 28 post-transfer. **f**) TAM:engineered T cell ratio in PDA. **g**) Representative flow cytometric plots of cytokine production of TCR$_{Msln}$ T cells isolated at day 8 post infusion from tumor and spleen of a *KPC* mouse treated with anti-CD115. Plots are gated on donor (CD8$^+$Thy1.1$^+$) T cells. **h**) Frequency of IFNγ^+ engineered T cells isolated from spleen

(Spl) or tumor (Tu) following a 5-hour *in vitro* stimulation with antigen on day 8 or day 28 post T-cell infusion. **i**) Frequency of TCR_{Msln}-engineered T cells that express PD-1 at 8 and 28 days post infusion. Figures a-i represent 3–4 mice/group from 2 independent experiments. **j**) Frequency (left) and number (right) of myeloid subsets in *KPC* PDA after T-cell infusion at survival endpoint. These cohorts were described previously (6) and each dot represents an independent mouse. Left panel is gated on $CD45^+CD11b^+$ cells. **k**) Correlation between frequency of $Ly6C^{high}$ TAMs and mouse survival. Data are mean ± SEM. *, $p<0.05$; **, $p<0.005$; and ***, $p<0.0001$ as determined by two-tailed unpaired Student's *t* test.

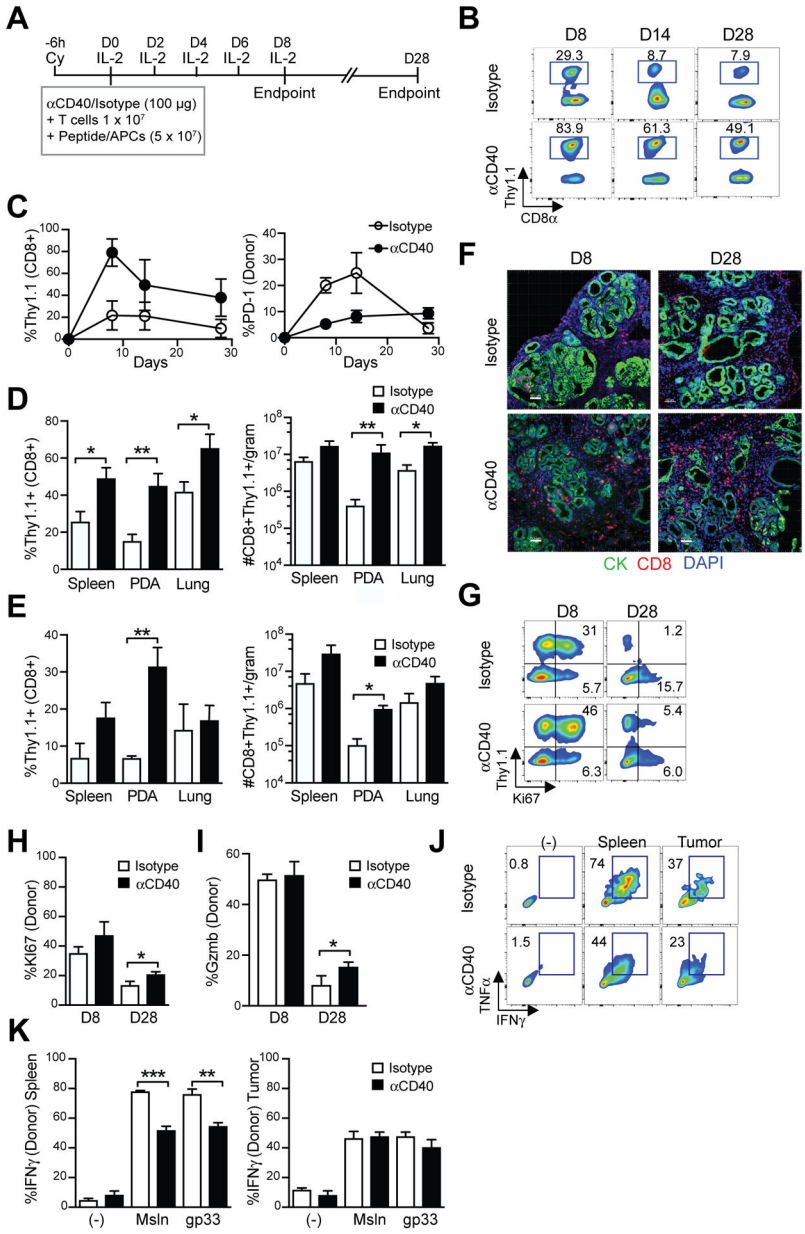

Figure 4. A single dose of anti-CD40 promotes TCR_{Msln}-engineered T-cell accumulation and persistence in PDA.

a) Treatment schematic of anti-CD40 and T-cell therapy. **b**) Representative flow cytometric plots of the frequency of engineered T cells ($CD8^+Thy1.1^+$) in the blood of *KPC* mice following infusion in mice that received anti-CD40 or isotype control. **c**) Quantification of engineered T cells ($CD8^+Thy1.1^+$) and PD-1 expression by engineered T cells (right graph) in blood. Plots are gated on $CD8^+$ T cells. **d**) Frequency (left) and number (right) of engineered T cells in spleen, tumors, and lung normalized to gram of tissue at 8 days post transfer. **e**) Frequency (left) and number (right) of engineered T cells in spleen, tumors and lung normalized to gram of tissue at 28 days post transfer. **f**) Representative staining for CD8 (red) and tumor cytokeratin (green) in autochthonous PDA. Scale bar, 50 μm. **g**) Representative flow cytometric plots of Ki67 expression in T cells in PDA. Gated on

$CD45^+CD8^+$ T cells. **h**) Frequency of donor T cells that express Ki67 in PDA. **i**) Frequency of donor T cells that express granzyme B (Gzmb) in PDA. Data is gated on $CD8^+Thy1.1^+$ donor T cells. Data are mean ± SEM. *, $p<0.05$; **, $p<0.005$; and ***, $p<0.0001$ as determined by two-tailed unpaired Student's *t* test. **i**) Granzyme B expression by engineered T cells in PDA at day 8 post T-cell transfer. **j**) Representative flow cytometric plots of cytokine production gated on donor T cells following *ex vivo* restimulation with peptide in the presence of a protein transport inhibitor. **k**) Quantification of cytokine production by engineered T cells in response to stimulation via the introduced TCR (Msln peptide), or the endogenous P14 TCR (gp33 peptide). Data are mean ± S.E.M. and representative of 3–6 mice/group. *, $p<0.05$; **, $p<0.005$; ***, $p<0.0005$ using two-tailed unpaired Student's *t* test. All data reflect 2 independent experiments.

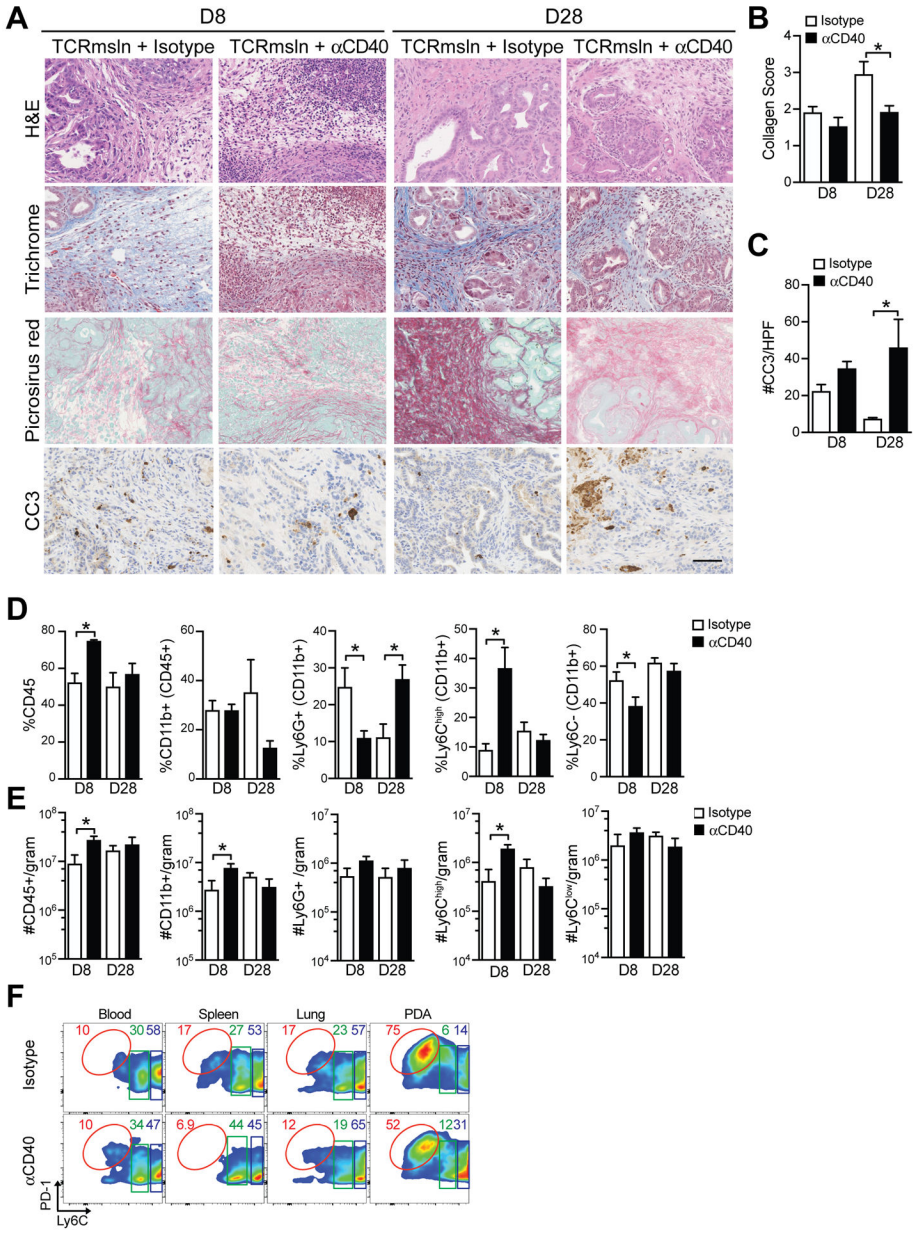

Figure 5. Impact of anti-CD40 and TCR$_{Msln}$ cell therapy in autochthonous PDA.

a) Histological staining of tumors from *KPC* mice. Scale bar, 25 μm. **b**) Collagen score of tumors following treatment with T cells ± anti-CD40. **c**) Number of tumor cells that express cleaved-caspase 3 (CC3) post T-cell therapy ± anti-CD40. **d**) Frequency of the indicated cell subset in autochthonous PDA post-T cell therapy. Myeloid subsets are gated are gated on CD45^{+}CD11b^{+} cells. **e**) Number of indicated cell subsets in autochthonous PDA post-T cell therapy. **f**) Representative flow cytometric plots of TAM subsets (gated on CD45^{+}CD11b^{+}Ly6G^{-}) cells in PDA at day 8 post therapy. All data reflect n=3–6 mice/group and 2 independent experiments. Data are mean ± SEM. *, $p<0.05$ using two-tailed unpaired Student's *t* test.